Published OnlineFirst November 10, 2020; DOI: 10.1158/0008-5472.CAN-20-1488

Frizzled-7 Identifies Platinum-Tolerant Ovarian Cancer Cells Susceptible to Ferroptosis

Yinu Wang[1], Guangyuan Zhao[1], Salvatore Condello[2], Hao Huang[1], Horacio Cardenas[1], Edward J. Tanner[1], JianJun Wei[3,4], Yanrong Ji[5], Junjie Li[6], Yuying Tan[6], Ramana V. Davuluri[5], Marcus E. Peter[4,7], Ji-Xin Cheng[6], and Daniela Matei[1,4,8]

ABSTRACT

Defining traits of platinum-tolerant cancer cells could expose new treatment vulnerabilities. Here, new markers associated with platinum-tolerant cells and tumors were identified using *in vitro* and *in vivo* ovarian cancer models treated repetitively with carboplatin and validated in human specimens. Platinum-tolerant cells and tumors were enriched in $ALDH^+$ cells, formed more spheroids, and expressed increased levels of stemness-related transcription factors compared with parental cells. Additionally, platinum-tolerant cells and tumors exhibited expression of the Wnt receptor *Frizzled-7* (*FZD7*). Knockdown of FZD7 improved sensitivity to platinum, decreased spheroid formation, and delayed tumor initiation. The molecular signature distinguishing $FZD7^+$ from $FZD7^-$ cells included epithelial-to-mesenchymal (EMT), stemness, and oxidative phosphorylation-enriched gene sets. Overexpression of FZD7 activated the oncogenic factor *Tp63*, driving upregulation of glutathione metabolism pathways, including glutathione peroxidase 4 (GPX4), which protected cells from chemotherapy-induced oxidative stress. $FZD7^+$ platinum-tolerant ovarian cancer cells were more sensitive and underwent ferroptosis after treatment with GPX4 inhibitors. *FZD7*, *Tp63*, and glutathione metabolism gene sets were strongly correlated in the ovarian cancer Tumor Cancer Genome Atlas (TCGA) database and in residual human ovarian cancer specimens after chemotherapy. These results support the existence of a platinum-tolerant cell population with partial cancer stem cell features, characterized by FZD7 expression and dependent on the FZD7–β-catenin–Tp63–GPX4 pathway for survival. The findings reveal a novel therapeutic vulnerability of platinum-tolerant cancer cells and provide new insight into a potential "persister cancer cell" phenotype.

Significance: Frizzled-7 marks platinum-tolerant cancer cells harboring stemness features and altered glutathione metabolism that depend on GPX4 for survival and are highly susceptible to ferroptosis.

Introduction

Ovarian cancer is the leading cause of death from female gynecologic cancers. Although initially a highly chemoresponsive tumor (1), most patients with ovarian cancer experience tumor relapse, and recurrent, resistant ovarian cancer is fatal (2). "Persister" or drug-tolerant cells have been described as cells surviving cytotoxic drug exposure (3) and represent a reservoir for the outgrowth of drug-resistant clones. Recent studies in various cancers have reported the molecular signature of "persister" cells, including upregulation of stemness factors, mesenchymal-like gene expression, enrichment in glutathione peroxidase 4 (GPX4) and other genes related to lipid peroxidation, which antagonize ferroptosis, allowing cells to survive after cytotoxic drug exposure (3–5). Small-molecule inhibitors targeting GPX4 were shown to induce lipid peroxidation and eliminate tyrosine kinase receptor inhibitor-tolerant cells through ferroptosis (3). It has been suggested that "persister" cells share characteristics with cancer stem cells (CSC), but also have distinct traits. Specific markers to allow their identification and early targeting remain elusive. Here we sought to characterize the ovarian cancer "persister" phenotype.

Our and other previous studies showed that although chemotherapy is effective at cytoreducing the mass of heterogeneous cancer cells, residual tumors persist and are enriched in CSCs (6, 7). Ovarian CSCs share some of the normal stem cells' characteristics, including the ability to self-renew, differentiate, express specific stem cell–surface markers (6, 8, 9), and exhibit enhanced tumor initiation capacity (TIC; ref. 10). Importantly, ovarian CSCs possess a phenotype associated with drug resistance, including diminished apoptotic responses, increased efflux mechanisms, and antioxidation defense (4, 8, 11, 12). The boundaries between stemness and platinum-resistant (Pt-R) phenotypes remain blurry and, while an overlap exists, it is assumed that distinct pathways drive the two entities.

As platinum-tolerant (Pt-T) cancer cells drive tumor relapse, we aimed to identify specific markers, by using *in vitro* and *in vivo* models of repeated exposure to the cytotoxic agent. We observed that Pt-T cells and tumors contained an increased $ALDH^+$ cell population, expressing stemness-related transcription factors (TF), and able to form more spheroids compared with chemotherapy-naïve cells. We identified the Frizzled 7 receptor (FZD7) as a novel cell-surface marker significantly upregulated in the platinum-tolerant cell population. *FZD7* knockdown increased sensitivity to Pt, decreased spheroid formation, and inhibited TIC. $FZD7^+$ cells harbored a "persister cell"–like signature, including downregulated genes associated with

[1]Department of Obstetrics and Gynecology, Feinberg School of Medicine, Northwestern University, Chicago, Illinois. [2]Department of Obstetrics and Gynecology, Indiana University School of Medicine, Indianapolis, Indiana. [3]Department of Pathology, Feinberg School of Medicine, Northwestern University, Chicago, Illinois. [4]Robert H. Lurie Comprehensive Cancer Center, Chicago, Illinois. [5]Division of Health and Biomedical Informatics, Department of Preventive Medicine, Northwestern University, Chicago, Illinois. [6]Department of Physics, Boston University, Boston, Massachusetts. [7]Department of Medicine, Feinberg School of Medicine, Northwestern University, Chicago, Illinois. [8]Jesse Brown Veteran Affairs Medical Center, Chicago, Illinois.

Note: Supplementary data for this article are available at Cancer Research Online (http://cancerres.aacrjournals.org/).

Corresponding Author: Daniela Matei, Northwestern University, 303 E Superior Street, Chicago, IL 60610. Phone: 312-503-4853; Fax: 312-503-4853; E-mail: daniela.matei@northwestern.edu

Cancer Res 2021;81:384–99

doi: 10.1158/0008-5472.CAN-20-1488

DNA damage response, upregulated epithelial to mesenchymal (EMT) and stemness, and decreased expression of genes associated with oxidative phosphorylation. Expression of the antioxidant enzyme GPX4 was increased in FZD7$^+$ Pt-T cells, rendering them sensitive to treatment with GPX4 inhibitors. Mechanistically, *FZD7* caused activation of the transcriptional regulator, *Tp63*, which drove upregulation of glutathione metabolism genes, protecting cells from oxidative stress. In all, our results support the existence of a "persister" Pt-T cell population, sharing traits with CSCs, marked by upregulation of the receptor *FZD7* and harboring a dependency on *FZD7–β catenin–Tp63*–mediated GPX4 expression and antioxidant activity.

Materials and Methods

Human specimens

Deidentified high-grade serous ovarian tumors (HGSOC) and associated malignant ascites were collected and processed fresh from patients who provided written informed consent. Tumor tissues were enzymatically disassociated into single-cell suspensions and cultured as previously described (6, 8). A tissue microarray (TMA) was built from deidentified HGSOC specimens ($n = 23$) from patients who had undergone three to six cycles of platinum-taxane neoadjuvant chemotherapy [Institutional Review Board (IRB)-approved CSR protocol #1247]. Each specimen was entered in duplicate, and fallopian tube epithelium ($n = 6$) served as control. Patient characteristics are shown in Supplementary Table S1. Human subject studies were conducted in accordance with the Declaration of Helsinki and approved by the IRB (Northwestern University IRB#: STU00202468).

Cell lines and culture conditions

SKOV3 and OVCAR3 cells were purchased from the ATCC. OVCAR5 cells were a generous gift from Dr. Marcus Peter, Northwestern University, Chicago IL; COV362 cells were from Dr. Kenneth Nephew, Indiana University, Indianapolis, IN; immortalized human fallopian tube luminal epithelial cells (FT190) were from Dr. R. Drapkin of University of Pennsylvania, Philadelphia, PA; ref. (13). PEO1 and PEO4 cells were from Sigma-Aldrich. Cell culture conditions are in Supplementary Material. Low-passage cells were used, and all cell lines were tested to be pathogen and *Mycoplasma* negative (Charles River Research Animal Diagnostic Services).

Chemicals and reagents

RSL3 was purchased from Fisher Scientific (cat. #611810). ML210 (cat. #SML0521), cisplatin (cat. # 1134357), and carboplatin (cat. #C2538) were from Sigma-Aldrich. WNT3a was from Fisher Scientific (cat. # 5036WN010CF, R&D Systems), and IWR-1-endo was from Santa Cruz (sc-295215A).

In vitro development of Pt-R cells

To generate Pt-T ovarian cancer cells, SKOV3, OVCAR5, COV362, and OVCAR3 cells were treated with three or four repeated or increasing doses of cisplatin or carboplatin for 24 hours. Surviving cells were allowed to recover for 3 to 4 weeks before receiving the next treatment. Changes in resistance to platinum were estimated by calculating half maximal inhibitory concentration (IC_{50}) values as described below.

In vivo experiments

Animal studies were conducted according to a protocol (#IS00003060) approved by the Institutional Animal Care and Use Committee of Northwestern University and are described in Supplementary Material. Experiments using patient-derived xenograft (PDX) tumors were performed in the Developmental Therapeutics Core of the Lurie Cancer Center, as previously described (14) and following a similar protocol (see Supplementary Material).

Isolation of tumor cells

Tumors from patients or xenografts were minced and enzymatically dissociated in DMEM/F12 (Thermo Fisher Scientific, Ref #11320) containing collagenase (300 IU/mL, Sigma-Aldrich, cat. #C7657) and hyaluronidase (300 IU/mL, Sigma-Aldrich, cat. #H3506) for 2 to 4 hours at 37°C. The tissue digest was passed several times through a 16- to 18G needle using Cell Stripper (Corning, cat. #25–056-CI) to dissociate remaining cell aggregates. Red blood cell lysis used RBC lysis buffer (BioLegend, cat. #420301), followed by DNaseI (Sigma-Aldrich, cat. # DN25) treatment and filtering through a 40-μm cell strainer (Fisher Scientific, cat. #NC0147038) to yield single-cell suspension.

Aldefluor assay and flow cytometry

Aldehyde dehydrogenase (ALDH) activity was measured using an Aldefluor assay kit (STEMCELL Technologies, cat. #01700) following the manufacturer's instructions and as described previously (6).

Cell survival assay

Cell survival was measured with a Cell Counting Kit 8 (CCK8, Dojindo Molecular Technologies, cat. #CK04), following the manufacturer's protocol. Absorbances (450 nm) were measured with a microplate reader (BioTek ELX800, BioTeK).

Detailed protocols for spheroid formation assay, clonogenic assay, RNA extraction, quantitative RT-PCR, Western blotting and IHC are included in Supplementary Material. Primers are included in Supplementary Table S2.

Extreme limited dilution assay

A serial dilution of OVCAR5_shControl or OVCAR5_shFZD7 cells (5, 10, 50, 100, 500, 1,000, and 5,000 cells) was sorted by FACS directly into 96-well low-attached plates and cultured in MammoCult medium for 14 days as described above. Each dilution included 10 replicates. The total number of wells containing spheroids for each dilution were counted. The CSC frequency and statistical significance were determined using ELDA software at http://bioinf.wehi.edu.au/software/elda/ (15).

Half maximal inhibitory concentration (IC_{50})

The IC_{50} values of the various treatment compounds were determined by the CCK8 assay as described in Supplementary Material. IC_{50} values were determined by logarithm-normalized sigmoidal dose curve fitting using Prism 6 software (GraphPad Software Inc.).

Lipid peroxidation assay

Intracellular lipid peroxidation was determined by a lipid peroxidation assay (Sigma-Aldrich, cat. #MAK085) following the manufacturer's protocol (see Supplementary Material).

Oxygen consumption rate

Cells were seeded on 96-well plates at 100,000 cells/well and incubated overnight. Ten microliters of extracellular O_2 consumption reagent (Oxygen Consumption Rate Assay kit, Abcam cat. #197243)

Published OnlineFirst November 10, 2020; DOI: 10.1158/0008-5472.CAN-20-1488

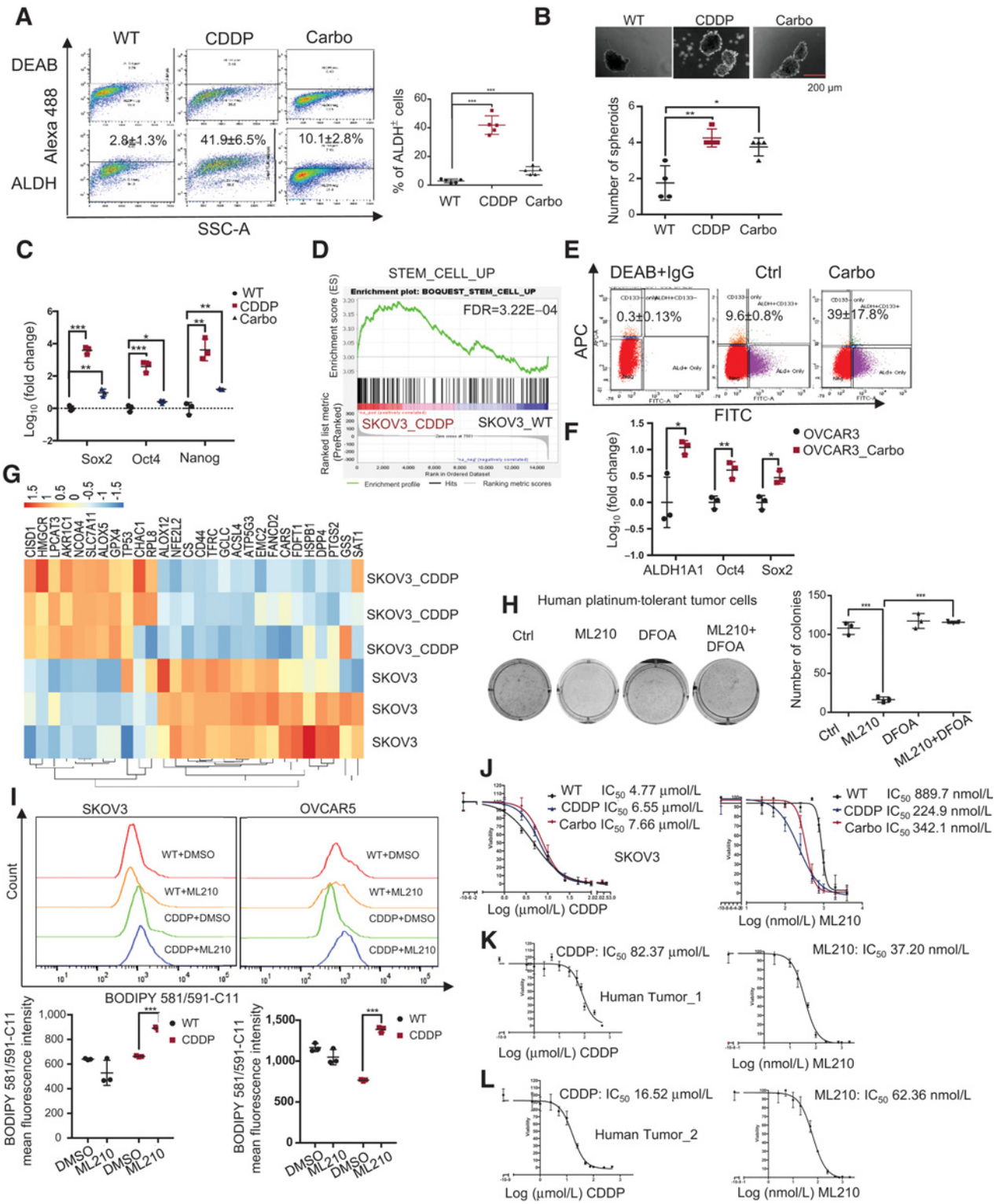

Figure 1.

Stemness and ferroptosis signatures are enriched in Pt-T ovarian cancer cells. **A,** Representative FACS side scatter analysis of the ALDH$^+$ population (left) and percentage (mean ± SD, $n = 5$) of ALDH$^+$ cells (right) in parental (WT), cisplatin-tolerant (CDDP), and carboplatin-tolerant (Carbo) SKOV3 cells. **B,** Representative images (top) and number (mean ± SD, $n = 4$) of spheroids (bottom) formed by 1,000 parental (WT), CDDP, and carboplatin-tolerant (Carbo) SKOV3 cells after 7 days of culture under non-attachment conditions. (*Continued on the following page.*)

Published OnlineFirst November 10, 2020; DOI: 10.1158/0008-5472.CAN-20-1488

was added to each well, and fluorescence was measured with a plate reader (SpectraMax i3X, Molecular Devices) at 3-minute intervals for 180 minutes at excitation/emission = 380/650 nm. Alternatively, oxygen consumption was measured using a Seahorse assay. Briefly, OVCAR5 shControl and shFZD7 cell lines were seeded in Seahorse 96-well microplate (Agilent, cat. #102416-100) at a density of 10–80K per well. After incubation overnight, oxygen consumption was measured and calculated by Seahorse XFe96 Analyzer (Agilent).

BODIPY staining for lipid peroxidation

Cells were treated as described in Supplementary Material. After treatment, cells were stained with BODIPY 581/591 C11 (5 μmol/L) for an hour at 37°C, washed with PBS, and fixed with 4% PFA on ice for 30 minutes. The mean fluorescence intensity (minimum of 10,000 events per condition) was measured by FACS (LSRFortessa, BD). BODIPY emission was recorded on channels for FITC at 520 nm and PE at 580 nm. The data were displayed as histograms, and mean fluorescence intensity of FITC was calculated.

Intracellular reactive oxygen species (ROS) levels were measured by monitoring the oxidation of cell-permeable 2′,7′-dichlorofluorescein diacetate (DCFHDA, Sigma-Aldrich) at excitation and emission wavelengths of 480 and 535 nm. 150,000 cells cultured in 35-mm glass bottom dish were treated with 1 or 2 μmol/L ML210 alone or with 800 nmol/L DFOA for 24 hours. Cell cultures were then treated with 10 μmol/L DCFDA (Abcam, cat. #ab113851) for 15 minutes to detect ROS level through confocal fluorescence microscopy. ROS level was measured as integral fluorescence intensity normalized by the cellular area in a frame (n = 15 frames) using ImageJ (https://imagej.nih.gov/ij).

RNA sequencing and data analysis

The RNA sequencing (RNA-seq) libraries (n = 3 per experimental group) were prepared using the NEBNext Ultra II RNA library prep kit from Illumina (New England Biolabs Inc.; see Supplementary Material). Trimmed reads were aligned to the ENSEMBL human genome version GRCh38 using STAR (2.5.2; ref. 16) and SAMtools (17). Mapped reads were then counted using HTSeq (18). Differentially expressed genes were determined by exact test analysis followed by multiple hypothesis correction using false discovery rate (FDR) on the edgeR package (19). Genes with FDR ≤ 0.05 were considered differentially expressed. Normalized counts for all genes were ranked and subjected to Gene Set Enrichment Analysis (20). Data are deposited in GEO (GSE148003).

Analysis of data from The Cancer Genome Atlas (TCGA) included correlation analysis between gene pairs and survival analysis, described in Supplementary Material.

Statistical analyses of experimental data

All data are presented as mean values ± SD of triplicate measurements. Two-tailed Student t test or ANOVA (one-way or two-way) were used to determine effects of treatments. $P < 0.05$ were considered significant. All analyses were performed using Prism 6.0 software (GraphPad Software).

Results

Stemness and ferroptosis signatures are enriched in platinum-tolerant cancer cells

Pt-T ovarian cancer cells were generated through repeated *in vitro* exposure of ovarian cancer cell lines (OVCAR3, OVCAR5, COV362, and SKOV3) to platinum at IC_{50} concentrations (Supplementary Fig. S1A), while Pt-R xenografts were obtained by treating tumor harboring mice with carboplatin for four to six weekly cycles (Supplementary Fig. S1B). Repeated platinum exposure of ovarian cancer cells induced a stable phenotype, with at least 2-fold increase in platinum IC_{50} (Supplementary Table S3) compared with parental chemotherapy-naïve cells. Pt-T ovarian cancer cells were enriched in $ALDH^+$ cells (**Fig. 1A**; Supplementary Fig. S2A), formed increased numbers of spheroids (**Fig. 1B**; Supplementary Fig. S2B), and contained cells expressing CSC-related TFs (*Oct4, Nanog,* and *Sox 2*; **Fig. 1C**; Supplementary Fig. S2C and S2D) compared with controls. RNA sequencing compared Pt-R versus parental naïve cells, with transcriptomic signatures revealing enrichment in stemness-associated gene sets (**Fig. 1D**; Supplementary Fig. S2E). Similar observations were made *in vivo*, including in carboplatin-treated OVCAR3 (**Fig. 1E** and **F**) and SKOV3 (Supplementary Fig. S2F) xenografts. $ALDH^+$ cells were enriched (**Fig. 1E**) and stemness-associated genes (*ALDH1A1, Oct4, Nanog,* and *Sox 2*) were upregulated (**Fig. 1F**; Supplementary Fig. S2F) in carboplatin-treated compared with PBS-treated xenografts, as we noted previously (6, 7).

Given the possibility that CSCs would be more resistant to chemotherapy due to upregulated antiredox mechanisms (11) and considering a recently proposed association between oxidative stress and ferroptosis, a new form of cell death triggered by oxidized lipids, we examined a gene set related to "ferroptosis" (21) in Pt-T compared with parental ovarian cancer cells. Clear differences including upregulated genes involved in glutathione metabolism and antioxidant defense mechanisms were observed in Pt-T ovarian cancer cells versus chemotherapy-naïve cells (SKOV3, **Fig. 1G**; OVCAR5, Supplementary Fig. S2G). Interestingly, this molecular signature was observed in HGSOC cells with higher baseline resistance to platinum (IC_{50} >5 μmol/L; COV362, OVCAR8, SNU119, and OVCAR4) compared with cells more sensitive to platinum (IC_{50} <5 μmol/L; TYKNU, IGROV1, OVCAR3; Supplementary Fig. S2H; refs. 7, 22), suggesting the pathway is a common signature of Pt-resistant cells. The selenoprotein glutathione peroxidase 4 (*GPX4*), a key protein regulating antioxidant response, was among the upregulated genes in Pt-T cells. GPX4 inhibitors impede antioxidant defense mechanisms and promote death of cells dependent on this pathway (3). Indeed, Pt-R

(*Continued.*) **C,** mRNA levels (fold change ± SD, n = 3) of stemness-related TFs (*Sox2, Oct4,* and *Nanog*) measured by real-time RT-PCR in CCDP- and Carbo-tolerant vs. parental SKOV3 cells (WT). **D,** GSEA shows upregulated stemness pathway (Stem Cell_UP) in SKOV3 CDDP-tolerant vs. parental cells (FDR = 3.22E−04). **E** and **F,** FACS side scatter analysis of percentage of $ALDH^+$ cells (**E**) and fold change (mean ± SD, n = 3) *ALDH1A1, Nanog*, and *Oct4* mRNA expression levels (**F**) in OVCAR3 xenografts treated with PBS (Ctrl) or carboplatin (Carbo). **G,** Hierarchical clustering heat map for DEG (FDR < 0.05) ferroptosis-related genes in SKOV3_CDDP vs. control cells (n = 3 replicates/group). **H,** Representative pictures of a colony formation assay (left) and number (mean ± SD, n = 3) of colonies (right) developed from 4,000 cells isolated from Pt-R human tumors treated with DMSO (Ctrl), ML210 (500 nmol/L), DFOA (800 nmol/L), or ML210 plus DFOA for 24 hours. **I,** Fluorescence histograms (top) and mean (± SD, n = 3) fluorescence (bottom) of BODIPY 581/591-C11 staining show lipid peroxidation in SKOV3 and OVCAR5 parental (WT) cells and cisplatin-tolerant (CDDP) cells treated with DMSO or ML210 (1 μmol/L) for 20 hours. **J,** Survival curves for WT, cisplatin-tolerant (CDDP), and carboplatin-tolerant (Carbo) SKOV3 cells in response to cisplatin (left) or GPX4 inhibitor ML210 (right). Cisplatin and ML210 IC_{50} values are shown. **K** and **L,** Survival curves of cells from primary HGSOC tumors treated with cisplatin (left) or GPX4 inhibitor ML210 (right). IC_{50} for cisplatin and ML210 are shown. For all comparisons: *, $P < 0.05$; **, $P < 0.01$; ***, $P < 0.001$.

Published OnlineFirst November 10, 2020; DOI: 10.1158/0008-5472.CAN-20-1488

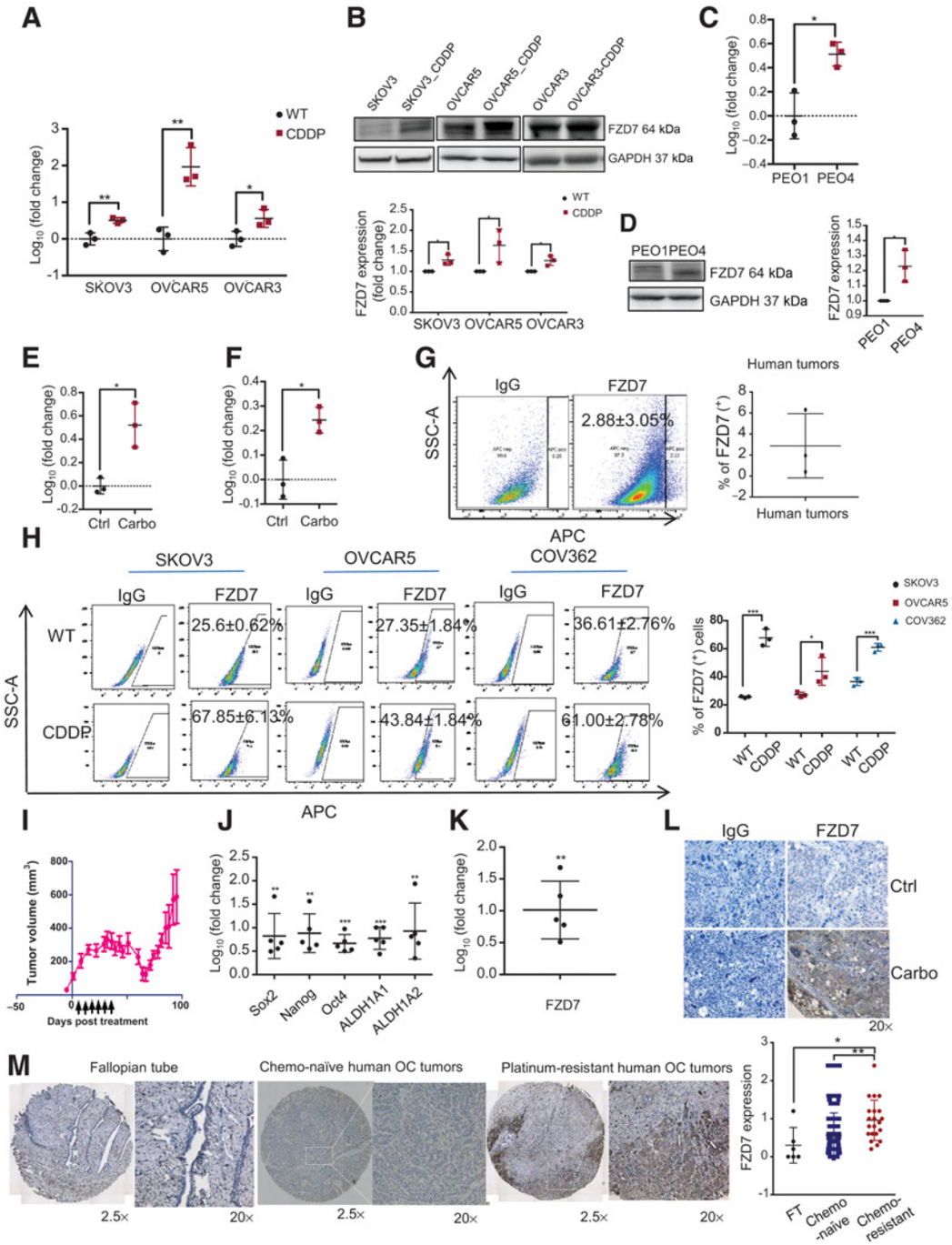

Figure 2.

Frizzled 7 (FZD7) is upregulated in Pt-T ovarian cancers. **A,** Fold change (mean ± SD, $n = 3$) of *FZD7 mRNA* expression levels measured by real-time RT-PCR in cisplatin-tolerant (CDDP) compared with parental OVCAR3, OVCAR5, and SKOV3 cells. **B,** Western blotting for FZD7 in parental and Pt-T SKOV3, OVCAR5, and OVCAR3 cells and Pt-T (-CDDP). Quantification shows fold change of FZD7 expression ($n = 3$ experiments). **C** and **D,** *FZD7 mRNA* expression levels (mean fold change ± SD, $n = 3$; **C**), and FZD7 protein levels measured by Western blotting (**D**; including quantification in three experiments) in Pt-R PEO4 vs. PEO1 cells. **E,** Fold change (mean ± SD) of *FZD7 mRNA* levels in carboplatin-treated (Carbo) and control (Ctrl) SKOV3 (**E**) and OVCAR3 (**F**) xenografts ($n = 3$ per group). **G,** FACS side scatter analysis (left) and average (±SD, $n = 3$) of FZD7$^+$ cells dissociated from HGSOC tumors. **H,** FACS side scatter analysis of FZD7$^+$ cells (left) and percentage (mean ± SD, $n = 3$) of FZD7$^+$ cells (right) in WT and Pt-T SKOV3, OVCAR5, and COV362 cells. **I,** NSG mice carrying PDX received carboplatin (15 mg/kg weekly) to induce platinum tolerance. Arrows, carboplatin treatment. Mean volumes (± SD) are shown ($n = 5$). **J,** Mean fold change (± SD, $n = 5$) for *Sox2, Nanog, Oct4, ALDH1A,* and *ALDH1A2 mRNA* expression levels in Pt-T vs. control PDXs. **K** and **L,** Mean fold change of *FZD7* mRNA levels (**K**) and representative images of FZD7 IHC staining (**L**) in Pt-T vs. control PDXs (Ctrl). **M,** FZD7 IHC staining and H-scores (mean ± SD; right) in sections of fallopian tube ($n = 6$), chemo-naïve ovarian cancer tumors ($n = 117$), and Pt-T tumors ($n = 23$) included in two tissue microarrays. For all comparisons: *, $P < 0.05$; **, $P < 0.01$; ***, $P < 0.001$.

Published OnlineFirst November 10, 2020; DOI: 10.1158/0008-5472.CAN-20-1488

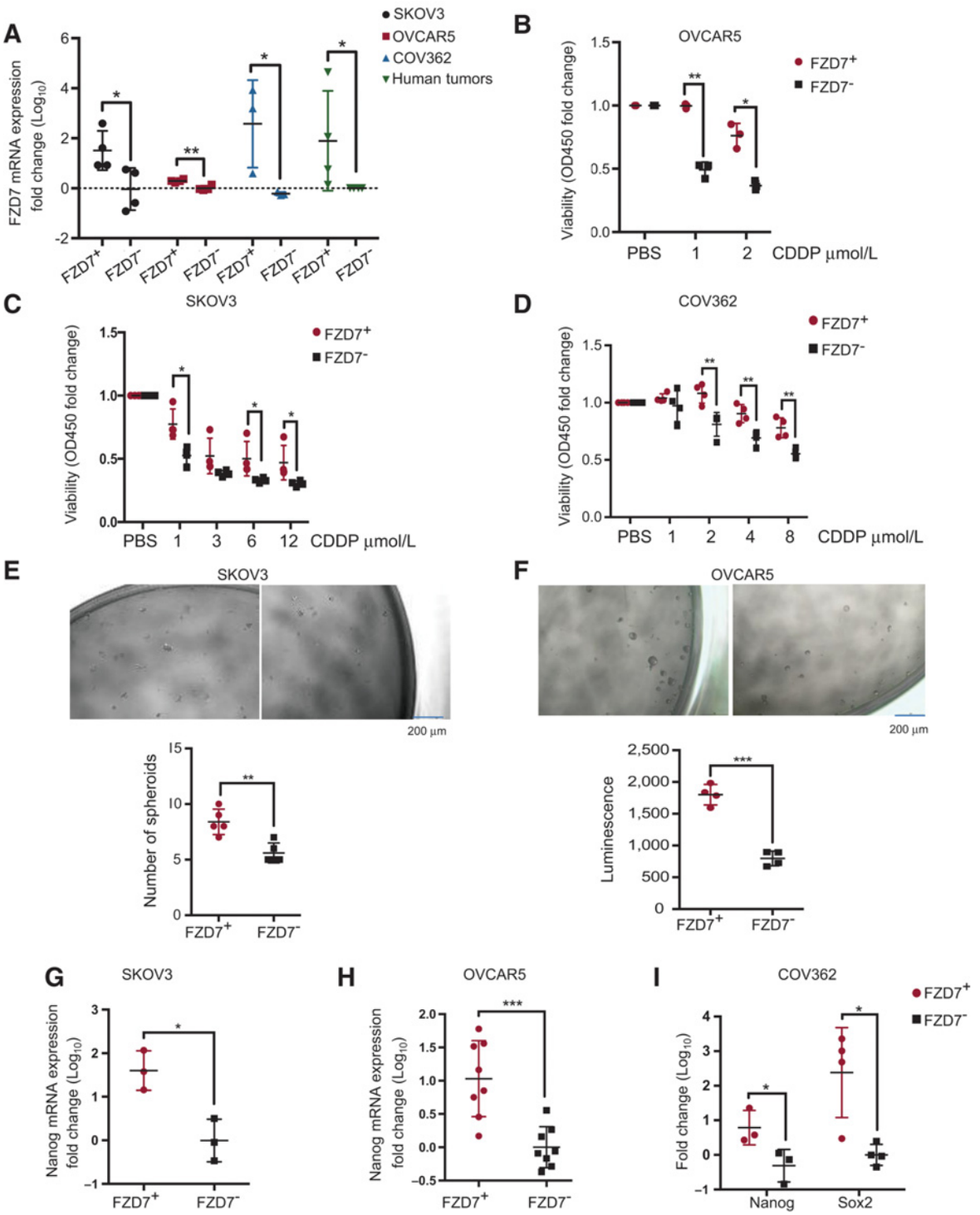

Figure 3.

Functional role of FZD7 in ovarian cancer cells. **A,** *FZD7 mRNA* levels (mean fold change ± SD, $n = 3$–4) in FZD7 $^{+}$ and FZD7 $^{-}$ cells FACS selected from SKOV3, OVCAR5, and COV362 cells and HGSOC tumors. **B–D,** Cell viability (mean fold change ± SD, $n = 4$) of FZD7^{+} and FZD7^{-} cells from OVCAR5 ($n = 3$; **B**), SKOV3 ($n = 3$; **C**), or COV362 ($n = 4$; **D**) cells, plated, treated with the indicated doses of CDDP for 24 hours, and cultured for additional 3 days. **E** and **F,** Representative pictures and numbers (mean ± SD, $n = 4$–5) of spheroids formed after 7 days of culture by FZD7^{+} and FZD7^{-} cells FACS sorted from SKOV3 (**E**) and OVCAR5 (**F**) ovarian cancer cells. Spheroids were counted or cell numbers were estimated by CellTiter-Glo 3D cell viability assay. **G–I,** mRNA levels (fold change ± SD) of *Nanog* in FZD7^{+} compared with FZD7^{-} cells from SKOV3 ($n = 3$; **G**), OVCAR5 ($n = 8$; **H**), and COV362 ($n = 3$; **I**) cells. For all comparisons: *, $P < 0.05$; **, $P < 0.01$; ***, $P < 0.001$.

Published OnlineFirst November 10, 2020; DOI: 10.1158/0008-5472.CAN-20-1488

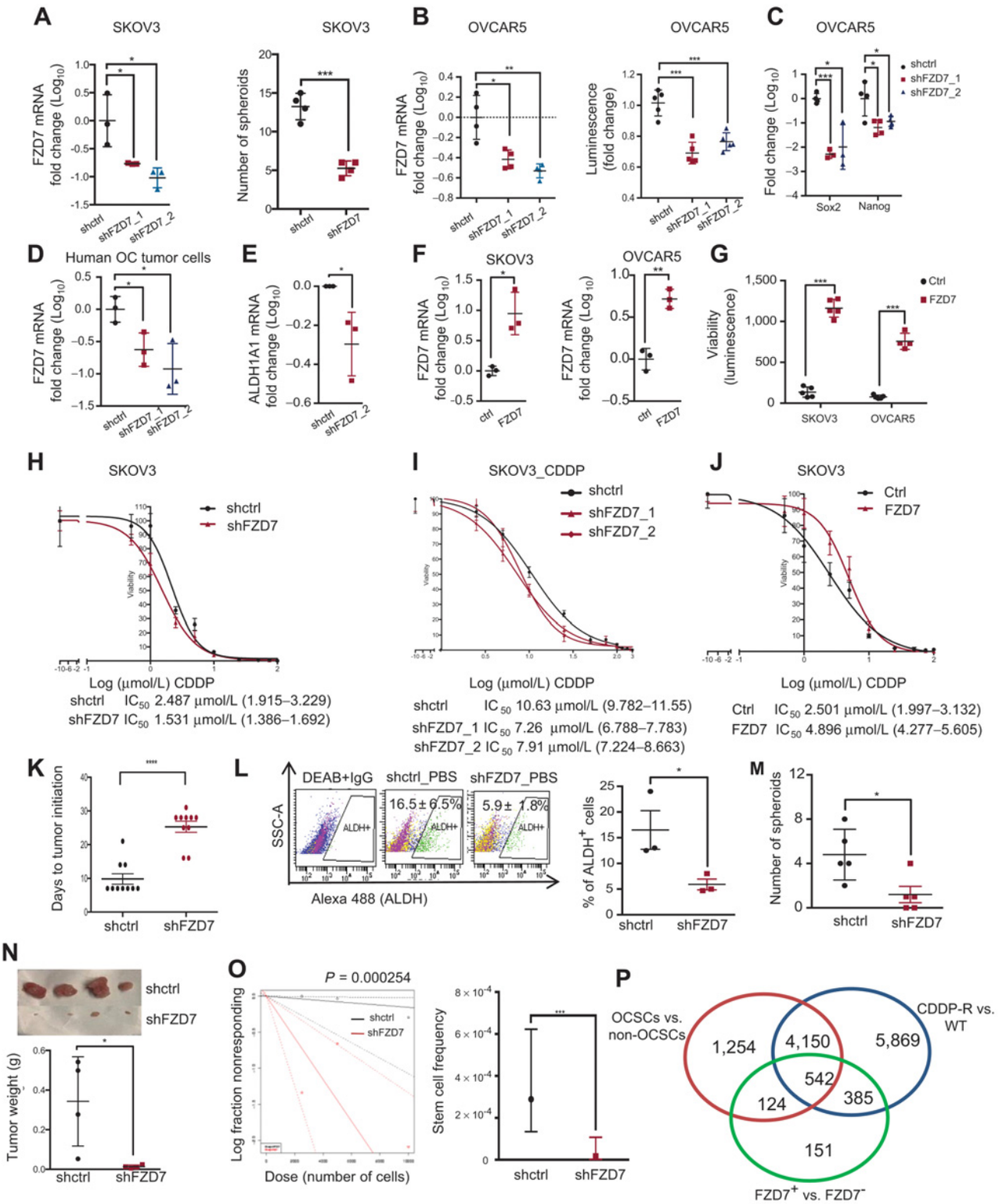

Figure 4.

FZD7 regulates stemness characteristics. **A,** Left, *FZD7 mRNA* levels (mean fold change ± SD, $n = 3$) in SKOV3 cells transduced with shRNAs targeting *FZD7* (shFZD7) vs. control shRNAs (shctrl). Right, number of spheroids (mean ± SD, $n = 4$) formed by 2,000 shFZD7 or shctrl SKOV3 cells cultured for 14 days and counted under a microscope. (*Continued on the following page.*)

Published OnlineFirst November 10, 2020; DOI: 10.1158/0008-5472.CAN-20-1488

ovarian cancer cells were more sensitive to the GPX4 inhibitor, ML210, compared with control cells (SKOV3, Supplementary Fig. S3A; OVCAR5, Supplementary Fig. S3B; COV362, Supplementary Fig. S3C). ML210-induced inhibition of colony formation was inhibited by the iron chelator deferoxamine (DFOA), consistent with induction of a ferroptosis phenotype (Supplementary Fig. S3A–S3C). Furthermore, primary ovarian cancer cells derived from malignant ascites from patients with Pt-R ovarian cancer were found to be dependent on GPX4, as ML210 potently reduced colony formation in these cells (**Fig. 1H**), this inhibition being rescued by DFOA.

ML210 caused increased oxidized membrane lipid levels, as measured by flow cytometry using the C11-BODIPY dye in Pt-T cells compared with naïve cells, supporting increased susceptibility to ferroptosis of Pt-R ovarian cancer cells (SKOV3 and OVCAR5, **Fig. 1I**; COV362, Supplementary Fig. S3D). Additionally, Pt-T SKOV3 cells were more sensitive to ML210 compared with parental cells (IC_{50} of 224 nmol/L and 342 nmol/L versus 889 nmol/L, **Fig. 1J**; Supplementary Fig. S3E and S3F). Primary ovarian cancer cells derived from malignant ascites associated with Pt-R ovarian cancer displayed resistance to platinum *in vitro* (**Fig. 1K** and **L**, left; IC_{50} of 82 and 16.52 μmol/L), and responded to low doses of the GPX4 inhibitors, ML210 (**Fig. 1K** and **L**, right; IC_{50} of 37.20 and 62.36 nmol/L) and RSL-3 (Supplementary Fig. S3G and S3H, IC_{50} of 14.20 and 17.72 nmol/L). Trypan blue staining of parental and Pt-T SKOV3 and OVCAR5 cells treated with ML210 showed that the inhibitor induced more cell death in resistant ovarian cancer cells ($P < 0.05$, Supplementary Fig. S3I and S3J). These results derived from multiple *in vitro* and *in vivo* ovarian cancer models, including primary human cancer cells, support the existence of a "persister cell" phenotype induced by Pt, sharing partial stemness characteristics, and highly susceptible to ferroptosis.

Frizzled-7 is upregulated in Pt-T ovarian cancer cells and tumors

To identify potential markers linked to the "persister" phenotype, an RT-PCR–based platform representing 90 cancer stemness-associated genes was used. A number of known CSC markers were found to be upregulated in the Pt-T cells (*CD44, PROM1,* and *SOX2*), along with membrane transporters known to be associated with Pt resistance (*ABCG2* and *ABCB5*), and regulators of EMT (*TGFBR1, SNAI1, BMP7, TWIST 1* and *2, SNAI 1* and *2*; see Supplementary Table S4). Among transcripts representing membrane proteins, which could potentially be used as novel markers, *Frizzled-7* (*FZD7*), a transmembrane receptor involved in canonical Wnt/β-catenin/TCF and non-canonical Wnt/planar cell polarity signaling (23, 24), was one of the top highly expressed transcripts (> 8-fold) in Pt-R compared with control cells (Supplementary Table S4; Supplementary Fig. S4A). Increased *FZD7* expression levels were confirmed in Pt-T models (SKOV3, OVCAR5, and OVCAR3) generated as described, compared with control cells at *mRNA* (**Fig. 2A**) and protein level (**Fig. 2B**), but also in Pt-R PEO4 cells compared with sensitive PEO1 ovarian cancer cells, an isogenic cell line pair, derived from the same patient at different times during the disease course (**Fig. 2C** and **D**; ref. 25). Likewise, *FZD7 mRNA* expression levels were upregulated in platinum-treated SKOV3 (**Fig. 2E**) and OVCAR3 (**Fig. 2F**) xenografts compared with vehicle-treated tumors.

Flow cytometry was used to determine whether an FZD7 high ($FZD7^+$) cell population is detectable. $FZD7^+$ cells were detected among cells dissociated from primary ovarian cancer, previously untreated with chemotherapy, and represented ∼3% of all cells (**Fig. 2G**). In ovarian cancer cell lines, $FZD7^+$ cells were identified as a distinct subpopulation representing ∼25% to 35% of cells (SKOV3, OVCAR5, and COV362; **Fig. 2H**). Additionally, the $FZD7^+$ cell population was detectable and was enriched in Pt-T compared with parental cells (SKOV3, OVCAR5, and COV362; **Fig. 2H**), suggesting that this cell membrane receptor may be a marker of "persister" cells, preexisting in unselected cell populations prior to Pt exposure, and enriched after exposure to the drug.

Further, we used PDX generated from newly diagnosed HGSOC (14), which were treated weekly with carboplatin. After initial response, recurrent tumors emerged (**Fig. 2I**), which were enriched in $ALDH^+$ cells (Supplementary Fig. S4B), CSC-related TFs (*Sox 2, Nanog, Oct4),* as well as *ALDH1A1* and *ALDH1A2* (**Fig. 2J**). *FZD7* expression levels were upregulated at *mRNA* (**Fig. 2K**) and protein level (**Fig. 2L**), as measured by IHC in Pt-T PDX versus control. Next, IHC assessed FZD7 expression in primary HGSOC specimens and in tumors collected after three to six cycles of neoadjuvant chemotherapy, containing surviving cells after standard platinum-taxane treatment, which are presumably Pt-T. Patient characteristics are included in Supplementary Table S1. Increased FZD7 staining intensity (measured as H-score) was observed in cancer cells residual after chemotherapy in these specimens ($n = 23$), when compared with chemotherapy-naïve tumors ($n = 117$,

(*Continued.*) **B,** *FZD7 mRNA* expression levels (mean fold change ± SD, $n = 4$; left) and number of spheroids ($n = 5$; right) in OVCAR5 cells transduced with shRNAs directed at *FZD7* (shFZD7) vs. control shRNAs (shctrl). Cell viability assessed numbers of cells growing as spheroids using the CellTiter-Glo kit. **C,** *Sox2* and *Nanog* mRNA levels (mean fold change ± SD; $n = 3$–4) in OVCAR5 cells transduced with shFZD7 vs. shctrl. **D,** *FZD7 mRNA* levels (mean fold change ± SD, $n = 3$) in Pt-R primary HGSOC cells transduced with shRNAs targeting *FZD7* (shFZD7) vs. control shRNA (shctrl). **E,** *ALDH1A1* mRNA levels (mean fold change ± SD, $n = 3$) in primary tumor cells transduced with shFZD7 cells vs. shctrl. **F,** Average fold change (± SD, $n = 3$) of *FZD7 mRNA* in SKOV3 (left) and OVCAR5 (right) cells transfected with FZD7-pcDNA3.1 vs. empty vector (ctrl). **G,** Spheroid formation estimated with a CellTiter-Glo viability kit (bottom) from 1,000 ctrl and FZD7 expressing SKOV3 or OVCAR5 cells (described in **F**) and cultured for 7 days ($n = 4$–5 per group). **H–J,** Effects of CDDP on cell survival measured by CCK8 assays in SKOV3_shctrl and SKOV3_shFZD7 (**H**), SKOV3 cisplatin-tolerant cells (SKOV3_CDDP) transduced with shRNAs targeting FZD7 (shFZD7_1, _2) or control shRNA (**I**), and SKOV3 cells transfected with FZD7-pcDNA3.1 (FZD7) or empty vector (Ctrl; **J**). Cells were treated with cisplatin for 24 hours and cultured for additional 3 days ($n = 3$–4). Cisplatin IC_{50} value is shown. **K,** Days to tumor initiation (mean ± SD, $n = 10$) of subcutaneous xenografts induced by 2×10^6 shctrl and shFZD7-transduced OVCAR5 cells. **L,** FACS side scatter analysis of $ALDH^+$ cells (top) and percentage (mean ± SD, $n = 3$) of $ALDH^+$ cells (bottom) from cell suspensions generated from OVCAR5_shctrl and OVCAR5_shFZD7 xenografts. **M,** Number (mean ± SD, $n = 5$) of spheroids (bottom) formed during 14 days by 1,000 cells derived from cell suspensions from OVCAR5_shctrl or OVCAR5_FZD7 xenografts. **N** and **O,** *In vivo* limited dilution assay used serially diluted numbers (2,500, 5,000, and 10,000) of OVCAR5_shctrl and shFZD7 cells injected subcutaneously into nude mice ($n = 4$ replicates per group). **N,** Average tumor weights (±SD) are shown (for the 10,000 cells group). **O,** Stem cell frequencies were calculated by using the Extreme Limiting Dilution Analysis (http://bioinf.wehi.edu.au/software/elda/; $P = 0.000254$). **P,** A Venn diagram shows the number overlapping and unique DEGs between OVCAR5-derived OCSCs ($ALDH^+CD133^+$) versus non-OCSCs ($ALDH^-CD133^-$), OVCAR5 cisplatin tolerant (CDDP-R) vs. parental (WT), and $FZD7^+$ versus $FZD7^-$ OVCAR5 cells (FDR < 0.05). $ALDH^+CD133$/$ALDH^-CD133^-$ and $FZD7^+$/$FZD7^-$ cells were sorted by FACS. For all comparisons: *, $P < 0.05$, **, $P < 0.01$, ***, $P < 0.001$.

Published OnlineFirst November 10, 2020; DOI: 10.1158/0008-5472.CAN-20-1488

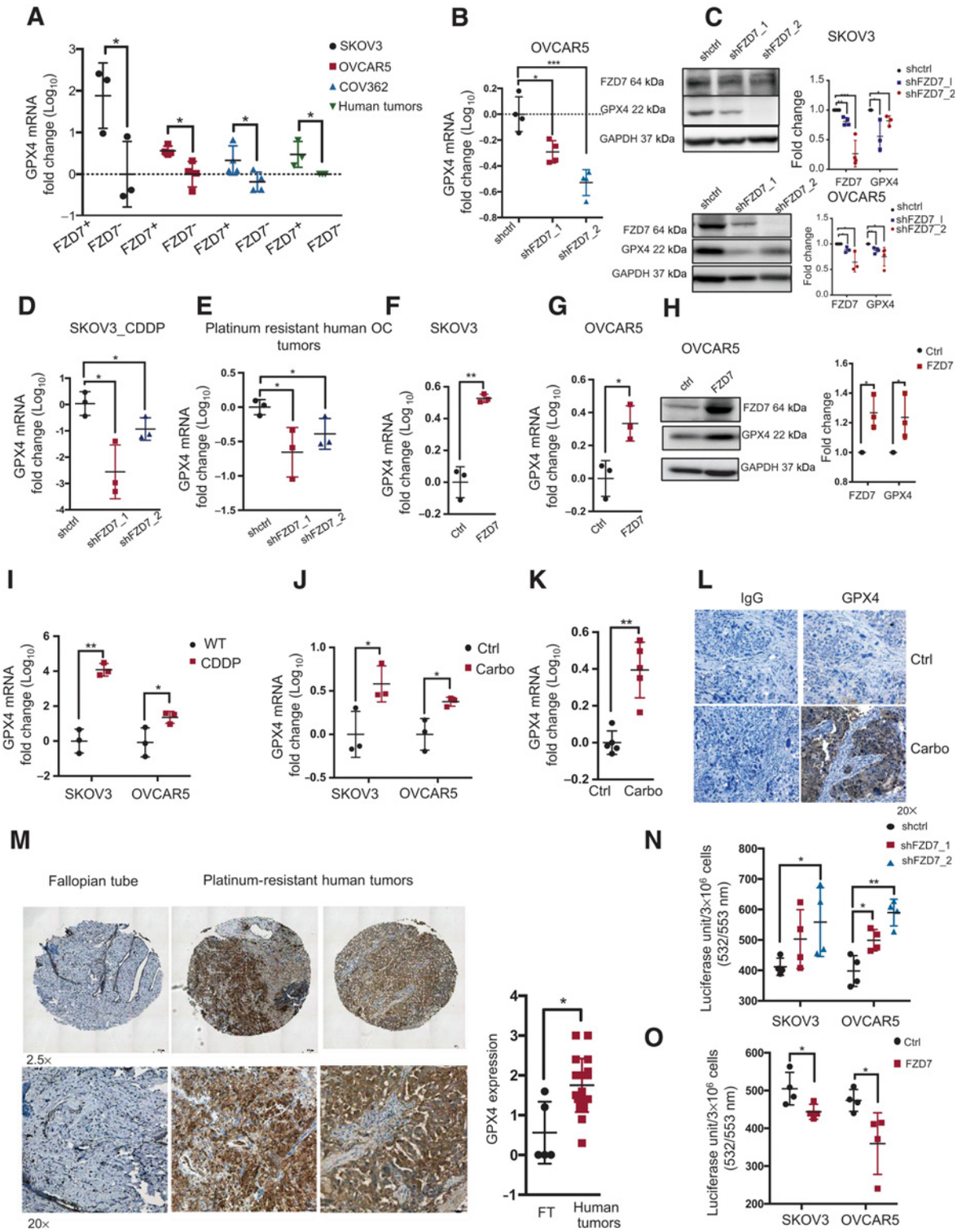

Figure 5.

FZD7 regulates GPX4 and intracellular redox states. **A,** Fold change (mean ± SD, $n = 3$–4) of *GPX4 mRNA* levels in FZD7$^+$ vs. FZD7$^-$ cells FACS sorted from SKOV3, OVCAR5, and COV362 cells and cell suspensions from HGSOC tumors. **B,** Fold change (mean ± SD, $n = 4$) of *GPX4 mRNA* expression levels in OVCAR5 cells transduced with shRNAs targeting *FZD7* (shFZD7) vs. control shRNAs (shctrl). **C,** Western blotting for FZD7, GPX4, and GAPDH in SKOV3 and OVCAR5 cells stably transduced with shctrl and shFZD7. (*Continued on the following page.*)

Published OnlineFirst November 10, 2020; DOI: 10.1158/0008-5472.CAN-20-1488

$P < 0.01$; ref. 26) and to fallopian tube epithelium (control $n = 6$, **Fig. 2M**, $P < 0.05$).

Functional role of FZD7 in ovarian cancer cells

$FZD7^+$ and $FZD7^-$ cells were FACS sorted from cell lines and human tumors. Differences in *mRNA* expression levels between $FZD7^+$ and $FZD7^-$ cell are shown in **Fig. 3A**. $FZD7^+$ovarian cancer cells were less sensitive to cisplatin (CDDP; **Fig. 3B–D**; $P < 0.05$), supporting that the receptor marks a Pt-T population. Additionally, $FZD7^+$ cells formed spheroids more efficiently compared with $FZD7^-$ cells (**Fig. 3E** and **F**, $P < 0.01$), and expressed higher levels of stemness-associated TFs (SKOV3, **Fig. 3G**, OVCAR5, **Fig. 3H**; COV362, **Fig. 3I**; $P < 0.05$), supporting that they share stemness-related features.

To further examine its functions, the receptor was knocked down (KD) by stable transduction of shRNA or was transiently overexpressed. Decreased *FZD7 mRNA* expression was confirmed by Q-RT-PCR in SKOV3 and OVCAR5 cells transduced with two shRNA sequences targeting the receptor (**Fig. 4A** and **B**). *FZD7* KD decreased spheroid formation (**Fig. 4A** and **B**) and expression of stemness-associated TFs (**Fig. 4C**; Supplementary Fig. S5A). *In vitro* serial limited dilution assay showed that receptor KD decreased stem cell frequency, as calculated by the ELDA software (27) in FZD7 KD versus control cells ($P = 0.034$, Supplementary Fig. S5B). Likewise, *FZD7* KD in Pt-T SKOV3_CDDP cells (Supplementary Fig. S5C) decreased sphere formation (Supplementary Fig. S5D). Stable *FZD7* KD in primary Pt-R tumor cells caused decreased expression levels of the stemness-associated gene *ALDH1A1* (**Fig. 4D** and **E**). Conversely, transient overexpression of *FZD7* (**Fig. 4E** and **F**) promoted proliferation of SKOV3 and OVCAR5 cells as spheres (**Fig. 4G**) and increased expression of stemness-associated TFs (Supplementary Fig. S5E and S5F). *FZD7* KD decreased IC_{50} to cisplatin by ∼2-fold (SKOV3, **Fig. 4H**; SKOV3_CDDP, **Fig. 4I**; Supplementary Fig. S5G and S5H), while the receptor's overexpression increased Pt resistance (**Fig. 4J**; Supplementary Fig. S5I).

To test the effects of FZD7 to tumor growth, a subcutaneous xenograft model was used. *FZD7* KD in OVCAR5 cells delayed tumor initiation (sh-control 9.8±4.6 days versus sh-FZD7 25.3±4.9 days, **Fig. 4K**, $P < 0.0001$) and decreased tumor size (Supplementary Fig. S5J) and tumor weight (0.80±0.41 g versus 0.14±0.15 g, $P = 0.04$, Supplementary Fig. S5K, $n = 4$/group). FZD7 KD in xenografts was confirmed by IHC (Supplementary Fig. S5L). $ALDH^+$ cells ($16.5\% \pm 6.5\%$ versus $5.9\% \pm 1.8\%$, $P = 0.05$; **Fig. 4L**, $n = 3$) and spheroid forming ability (**Fig. 4M**, $P = 0.02$) were decreased in cells dissociated from FZD7 KD versus control xenografts. Further, to test the effects of FZD7 KD to tumor initiation, an *in vivo* serial limited dilution assay was carried out by using 2,500, 5,000, and 10,000 FZD7 KD and control cells. FZD7 KD significantly inhibited TIC (**Fig. 4N**) and reduced stem cell frequency, as calculated by the ELDA software (**Fig. 4O**). Combined, these results support that FZD7 is linked to stemness and chemoresistance.

Molecular signatures of $FZD7^+$ cancer cells

Gene signatures distinguishing $FZD7^+$ versus $FZD7^-$ cells, ovarian CSCs ($ALDH^+CD133^+$) versus non-CSCs ($ALDH^-CD133^-$), and Pt-T versus platinum-naïve OVCAR5 cells were examined and integrated (**Fig. 4P**). $FZD7^+$ and $^-$ were sorted by FACS (Supplementary Fig. S5J). Ovarian CSCs and non-CSCs were FACS sorted by using dual stem cell markers, CD133 and Aldefluor activity (Supplementary Fig. S5M and S5N). There were 666 differentially expressed genes (DEG) shared between $FZD7^+$/$FZD7^-$ and CSCs/non-CSCs data sets, 5,404 DEGs being unique to CSCs and 536 DEGs unique to $FZD7^+$ cells (**Fig. 4P**). Additionally, there were 927 DEGs overlapping between $FZD7^+$/$FZD7^-$ and resistant/parental cells, 10,019 DEGs unique to the Pt-T cells, and 275 genes uniquely associated with $FZD7^+$ cells (**Fig. 4P**). Overlapping DEGs between $FZD7^+$/$FZD7^-$ and OCSC/non-OCSCs were enriched in cancer stem cell, but enriched DNA-repair signatures between $FZD7^{+/-}$ and resistant/parental cells (Supplementary Fig. S6A and S6B). Additionally, $FZD7^+$ versus $FZD7^-$ cells displayed signatures enriched in *stemness* (Supplementary Fig. S6C), *EMT* (Supplementary Fig. S6D) and *downregulated DNA damage response* genes (Supplementary Fig. S6E). Together, these data suggest that $FZD7^+$ cells possess both shared, but also distinct features, relative to stemness and chemoresistance, consistent with the phenotypes described above. Importantly, *mitochondrial and oxidative phosphorylation* gene sets were enriched among DEGs distinguishing $FZD7^+$ versus $FZD7^-$ cells (Supplementary Fig. S6F–S6H) and Ingenuity Pathway Analysis identified oxidative phosphorylation and mitochondria dysfunction as the top enriched pathways in $FZD7^+$ cells, suggesting that the receptor marks a cell population harboring altered oxidative stress responses.

FZD7 marks a cell population enriched in GPX4

Given that GPX4, an antioxidant enzyme that reduces ROS, preventing formation of toxic lipid peroxides (28, 29), has been implicated in maintenance of normal mitochondrial function and oxidative phosphorylation (3, 28), we examined whether *FZD7* expression affected *GPX4* expression and function in Pt-T ovarian cancer cells. *GPX4* levels were significantly increased in FACS-sorted $FZD7^+$ versus $FZD7^-$ cells derived from SKOV3, OVCAR5, and COV362 cells or cancer cells dissociated from human tumors (**Fig. 5A**, $P < 0.05$). Furthermore, *FZD7* KD by shRNA in OVCAR5 and SKOV3 cells resulted in repressed *GPX4 mRNA* (**Fig. 5B**, $P < 0.001$; Supplementary Fig. S7A, $P < 0.05$) and protein expression levels (**Fig. 5C**). GPX4 expression was decreased in Pt-T SKOV3 cells (**Fig. 5D**) and in primary Pt-R ovarian cancer cells (**Fig. 5E**) transduced with shRNA

(*Continued.*) Quantification shows fold change of FZD7 and GPX4 expression across three experiments. **D** and **E,** *GPX4 mRNA* expression levels (fold change ± SD, $n = 3$) in SKOV3 Pt-T cells (CDDP; **D**), and Pt-R primary human HGSOC cells (**E**) transduced with shRNAs directed at *FZD7* (shFZD7) vs. control shRNAs (shctrl). **F** and **G,** Average fold change (± SD, $n = 3$) of *GPX4 mRNA* levels in SKOV3 (**F**) and OVCAR5 (**G**) cells transfected with FZD7-pcDNA3.1 vs. empty vector (ctrl). **H,** Western blotting for FZD7, GPX4, and GAPDH in OVCAR5 cells transfected with FZD7-pcDNA3.1 vs. empty vector (ctrl). Quantification shows fold change of FZD7 and GPX4 expression across three experiments. **I–K,** *GPX4 mRNA* expression (mean fold change ± SD) in SKOV3 and OVCAR5 Pt-T (CDDP) vs. parental cells (WT; $n = 3$/group; **I**). **J,** SKOV3 and OVCAR5 xenografts ($n = 3$ per group; **J**) and PDX tumors ($n = 5$ per group; **K**) treated with PBS (Ctrl) or carboplatin. **L,** Representative images of GPX4 IHC staining in sections of control (Ctrl) and Pt-T PDXs. **M,** Representative pictures of GPX4 IHC (left) and H-scores (mean ± SD; right) in sections of fallopian tube ($n = 6$) and Pt-R HGSOC tumors ($n = 23$). **N,** Lipid peroxidation in SKOV3 and OVCAR5 cells transduced with scrambled shRNA (shctrl) or shRNAs targeting *FZD7* (shFZD7) and expressed as average luciferase units/3 × 10^6 cells (± SD, $n = 4$). **O,** Intracellular lipid peroxidation measured in SKOV3 and OVCAR5 cells transfected with FZD7 or control vector (Ctrl) and expressed as average luciferase units/3 × 10^6 cells ± SD ($n = 4$). For all comparisons: *, $P < 0.5$; **, $P < 0.01$; ***, $P < 0.001$.

Published OnlineFirst November 10, 2020; DOI: 10.1158/0008-5472.CAN-20-1488

targeting *FZD7*. Conversely, *FZD7* overexpression induced increased GPX4 *mRNA* and protein expression levels (**Fig. 5F–H**).

Furthermore, *GPX4* and *FZD7* mRNA expression levels were coordinately upregulated in Pt-T models, including Pt-T versus parental cells (SKOV3, OVCAR5, **Fig. 5I**, $P < 0.05$), Pt-T xenografts (**Fig. 5J**, $P < 0.05$) and PDXs (**Fig. 5K**, $P < 0.01$). Increased *GPX4* expression in Pt-T PDX versus controls was confirmed by IHC (**Fig. 5L**). IHC examined GPX4 in HGSOC specimens collected after neoadjuvant chemotherapy, noting increased GPX4 staining in these residual tumors ($n = 23$) when compared with fallopian tube epithelium, **Fig. 5M**, $P = 0.02$). Together, the results confirm a positive correlation between FZD7 and GPX4 expression in ovarian cancer cells and in Pt-T models, supporting that FZD7$^+$ cells have increased antioxidant capacity. To confirm the functional relevance, GPX4 enzymatic activity was measured by using the malondialdehyde (MDA) assay, which quantifies intracellular lipid peroxide levels. Lipid peroxides were found to be increased in *FZD7* KD versus control cells (**Fig. 5N**, $P < 0.05$) and decreased in ovarian cancer cells overexpressing *FZD7* (**Fig. 5O**, $P < 0.05$), supporting that FZD7$^+$ cells clear these toxic products more effectively, due to higher levels of GPX4.

GPX4 participates in regulation of intracellular redox states by utilizing glutathione (GSH) as the critical antioxidant (21). GSH is synthesized from glutamate–cysteine under the action of glutamate–cysteine ligase (GCL; ref. 21). The cycling of reduced GSH to oxidized glutathione disulfide (GSSG) removes ROS derived from hydrogen peroxide and lipid hydroperoxides through various glutathione peroxidases (GPX), including GPX4 (21). GSH recycling from GSSH is catalyzed by glutathione reductase (GSR), using NADPH, whose synthesis is regulated by isocitrate dehydrogenase 2 (IDH2; ref. 21). *FZD7* KD decreased the expression levels of multiple genes in this pathway, including *GPX2, GSS, IDH2, GSR, GCL,* and *SLC7A11* (OVCAR5, **Fig. 6A**; SKOV3, Supplementary Fig. S7B). Conversely, FZD7 overexpression caused increased expression levels of *GSS, GSR, GCL* and *SLC7A11* (OVCAR5, **Fig. 6B**; SKOV3, Supplementary Fig. S7C), suggesting a significant direct correlation between *FZD7* and glutathione metabolism-related genes.

FZD7 marks a cell population susceptible to GPX4 inhibitors

Given the correlations between FZD7, upregulated in Pt-T cells, and GPX4-mediated cellular redox maintenance, we hypothesized that inhibition of this axis will eliminate resistant cells. Small-molecule inhibitors of GPX4 have been shown to increase cellular oxidative stress and induce ferroptosis (3, 30–32). Thus, we examined the sensitivity of ovarian cancer cells with high versus low FZD7 expression levels to GPX4 inhibitors, ML210 and RSL3 (3, 32, 33). FZD7$^+$ sorted cells were more sensitive to the GPX4 inhibitor ML210 compared with FZD7$^-$ cells (OVCAR5, **Fig. 6C**; COV362, **Fig. 6D**, SKOV3, Supplementary Fig. S7D). *FZD7* KD in OVCAR5 and SKOV3 cells also slightly reduced sensitivity to GPX4 inhibitors (**Fig. 6E**; Supplementary Fig. S7E), while *FZD7* overexpression slightly increased sensitivity to ML210 compared with vector-transduced cells (**Fig. 6F**; Supplementary Fig. S7F).

Through its antioxidant function, GPX4 protects mitochondria from damage, maintaining normal oxidative phosphorylation. To test whether these processes were altered in FZD7$^+$ versus FZD7$^-$ cells, as a consequence of differential GPX4 expression, oxygen utilization was measured by using fluorescence-labeled oxygen uptake assay and the seahorse assays. FZD7 KD resulted in decreased oxygen uptake (Supplementary Fig. S7G) and consumption rate (Supplementary Fig. S7H), supporting the role of this pathway maintaining normal mitochondrial function. Additionally, intracellular ROS levels, quantified by DCFHDA staining, were decreased in *FZD7* KD cells compared with controls (**Fig. 6G**). As increased ROS levels contribute to oxidation of polyunsaturated lipids, leading to ferroptosis, C11-BODIPY staining was used in cells expressing different levels of FZD7 and/or exposed to GPX4 inhibitors. Oxidation of the polyunsaturated butadienyl portion of the dye in the presence of ROS is reflected in a shift of the fluorescence emission peaks from red to green, a hallmark of ferroptosis. The mean green (FITC) fluorescence intensity caused by oxidized lipids was decreased in cells overexpressing FZD7 and increased in FZD7 KD cells (**Fig. 6H**), consistent with increased susceptibility to ferroptosis of FZD7$^+$ cells. ML210-induced increase in fluorescence was higher in SKOV3 and OVCAR5 cells overexpressing FZD7 compared with controls and decreased in FZD7 KD cells (**Fig. 6I** and **J**). Likewise, baseline and ML210-induced intracellular ROS levels (rescued by DFOA) were higher in control versus FZD7 KD OVCAR5 cells (**Fig. 6K**). Collectively, the data suggest that cells marked by FZD7 are more susceptible to ferroptosis and could be eliminated by targeting GPX4.

FZD7 regulates GPX4 expression and glutathione metabolism by activating the canonical β catenin/p63 pathway

As a classic Wnt receptor, FZD7 participates in both canonical β-catenin and noncanonical signaling. One of the known β-catenin targets is the transcription factor *p63*, directly transactivated by the TCF/LEF complex (34). Its most common isoform, ΔNTp63, lacking its N-terminus domain, has been implicated in maintaining intracellular redox homeostasis by regulating genes involved in glutathione metabolism, including GPX4 (21). We therefore hypothesized that in Pt-T ovarian cancer cells, FZD7 could alter glutathione metabolism and protect ovarian cancer cells from oxidative stress, through activation of β-catenin/TP63 signaling. *Tp63* expression was upregulated in Pt-R PDX (**Fig. 7A**) and ovarian cancer cells compared with controls (Supplementary Fig. S8A). *Tp63* expression was higher in FZD7$^+$ versus FZD7$^-$ cells derived from SKOV3, OVCAR5, COV362, and human HGSOC (**Fig. 7B**), and FZD7 KD caused decreased *Tp63* expression in OVCAR5 (**Fig. 7C** and **D**) and SKOV3 cells (Supplementary Fig. S8B; **Fig. 7D**), while FZD7 overexpression led to increased Tp63 expression (**Fig. 7E–G**) at *mRNA* and protein levels. To demonstrate that the correlations between FZD7, TP63, and GPX4 were dependent upon the engagement of β-catenin, we used Wnt3A stimulation and the β-catenin inhibitor IWR-1-endo. Stimulation with Wnt3A induced p63 and GPX4 expression in control, but not in FZD7 KD, cells, while treatment with IWR-1-endo inhibited the expression of both p63 and GPX4 (**Fig. 7H**, OVCAR5 and S8F, SKOV3). Similar observations were made when FZD7 was overexpressed (Supplementary Fig. S8F), supporting that GPX4 upregulation is directly regulated by β-catenin.

Lastly, to determine whether FZD7 regulates GPX4 expression by altering Tp63 function, the effects of Tp63 knockdown on GPX4 expression in cells expressing high versus low levels of FZD7 were tested. Overexpression of *FZD7* and KD of *p63* in OVCAR5 cells was confirmed at the *mRNA* level (**Fig. 7I–K**; SKOV3, Supplementary Fig. S8C–S8E). *GPX4* upregulation induced by *FZD7* overexpression was abrogated in cells in which *p63* was KD (**Fig. 7K**; SKOV3, Supplementary Fig. S8E), supporting that this TF, engaged by β-catenin, downstream of *FZD7*, is an important regulator. Interestingly, *Tp63* KD caused reduced expression of *FZD7* in ovarian cancer cells transfected with either control vector or FZD7, indicating a feedback regulatory role of *Tp63* on *FZD7*. These experimental results were validated by examining the TCGA HGSOC database (35). *FZD7* and *Tp63* expression levels were positively correlated (**Fig. 7L**,

Published OnlineFirst November 10, 2020; DOI: 10.1158/0008-5472.CAN-20-1488

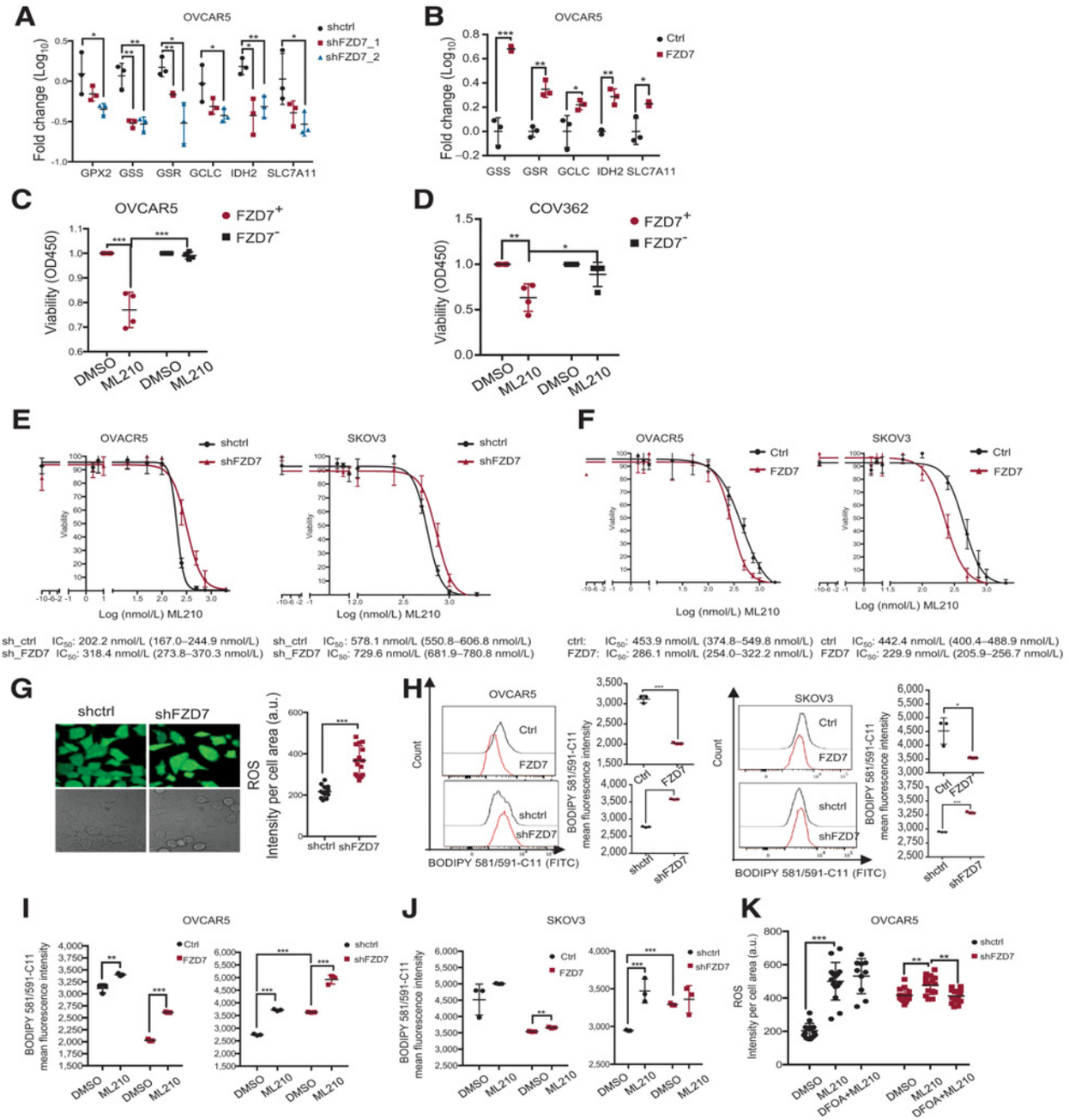

Figure 6.

FZD7 marks a cell population susceptible to GPX4 inhibitors. **A,** Average fold change (±SD, $n = 3$) in *mRNA* expression levels of selected glutathione metabolism genes in OVCAR5 cells transduced with shRNAs targeting FZD7 (shFZD7) vs. control shRNA (**A**) and in OVCAR5 cells transfected with FZD7-pcDNA3.1 (FZD7) vs. control vector (Ctrl; **B**). **C** and **D,** Viability of FZD7$^+$ and FZD7$^-$ cells sorted from OVCAR5 (**C**) and COV362 (**D**) cells and treated with DMSO or ML210 (OVCAR5, 2 μmol/L; COV362, 1 μmol/L) for 72 hours. Data are presented as average fold change (± SD, $n = 4$) of absorbance values relative to control. **E,** Survival curves of OVCAR5 (left) and SKOV3 (right) cells transduced with control shRNAs (shctrl) or shRNAs targeting *FZD7* (shFZD7) and treated with ML210 for 3 days ($n = 3$–4). ML210 IC_{50} values are shown below. **F,** Survival curves of OVCAR5 (left) and SKOV3 (right) cells transfected with FZD7-pcDNA3.1 or control vector and treated with ML210 for 3 days. ML210 IC_{50} values are shown below ($n = 3$–4). **G,** Images (left) and quantification (right) of intracellular ROS levels in OVCAR5 cells transfected with control shRNA (shctrl) or shRNA targeting *FZD7* (shFZD7). Data are presented as means (± SD) of DCF fluorescence intensity per cell area ($n = 15$). **H,** Histograms of fluorescence intensity (left) and mean (± SD, $n = 3$; right) of BODIPY 581/591-C11 in OVCAR5 (left) and SKOV3 (right) cells transfected with vector (ctrl), FZD7-pCDNA3.1 (FZD7), control shRNA (shctrl), or shRNAs targeting *FZD7* (shFZD7). **I** and **J,** Mean (± SD, $n = 3$) fluorescence intensity of BODIPY 581/591-C11 shows effects of ML210 (1 μmol/L for 20 hours) on lipid peroxidation levels in SKOV3 (**I**) and OVCAR5 (**J**) cells transfected with empty vector (ctrl), FZD7-pcDNA3.1 (FZD7), control shRNA (shctrl), or shRNA against *FZD7* (shFZD7). **K,** Intracellular ROS levels in OVCAR5 cells transfected with shctrl and shFZD7 treated with DMSO, ML210 (2 μmol/L, 24 hours), and ML210 + DFOA (800 nmol/L, 24 hours), measured by assessing DCFHDA oxidation. Average intensity per cell area (± SD) is shown ($n = 15$). For all comparisons: *, $P < 0.05$; **, $P < 0.01$; ***, $P < 0.001$.

Published OnlineFirst November 10, 2020; DOI: 10.1158/0008-5472.CAN-20-1488

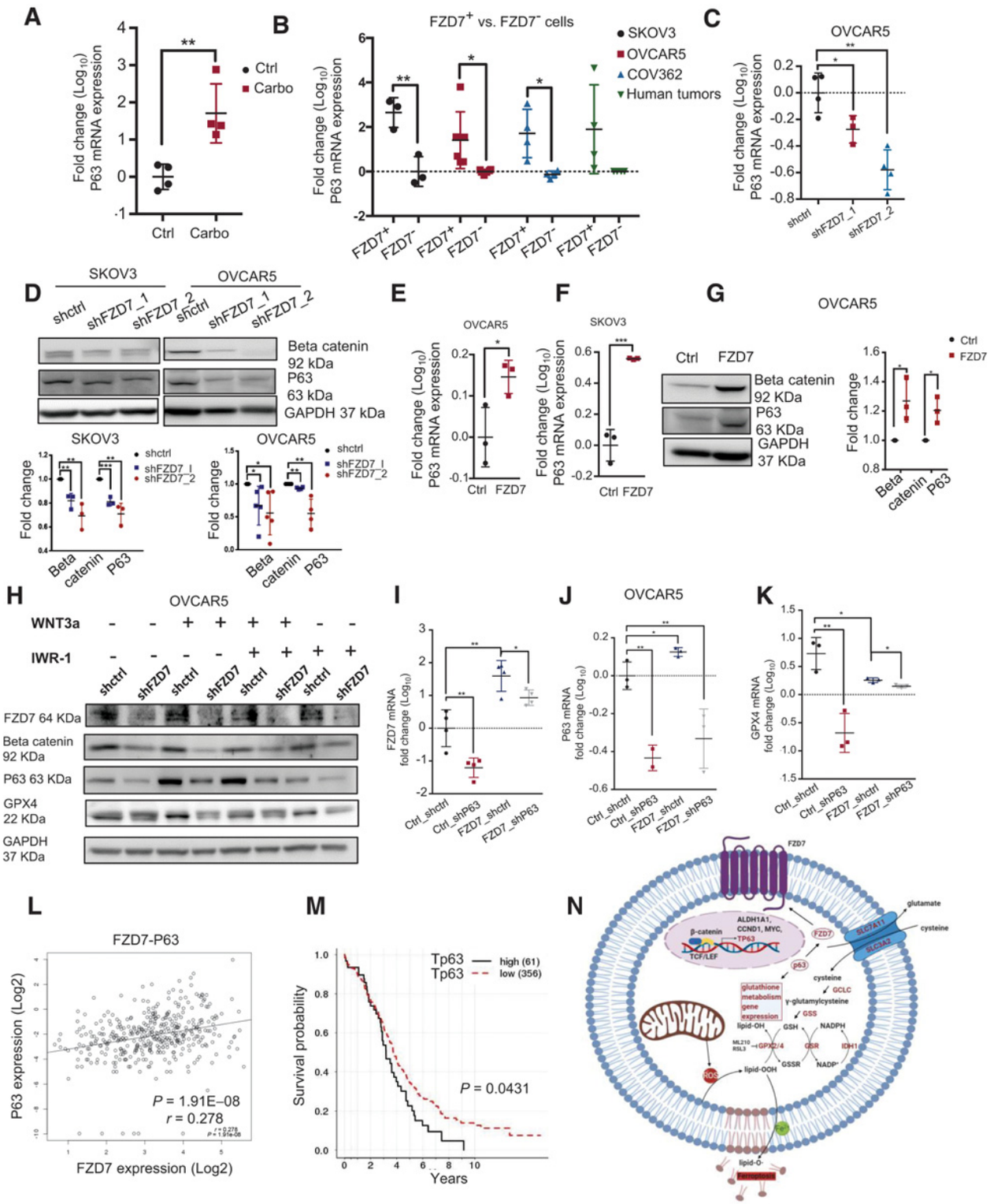

Figure 7.

FZD7 regulates GPX4 expression and gluthatione metabolism by activating the canonical β catenin/p63 pathway. **A,** *P63 mRNA* levels (fold change ± SD, $n = 4$) in Pt-T PDXs (carbo) vs. controls (Ctrl). **B,** *P63* mRNA levels (fold change ± SD, $n = 3$–6) in FZD7$^+$ versus FZD7$^-$cells sorted from SKOV3, OVCAR5, and COV362 cell lines, and cell suspensions from human tumors. **C,** *P63 mRNA* expression levels (fold change ± SD, $n = 4$) in OVCAR5 cells transduced with shRNAs targeting *FZD7* (shFZD7) vs. control shRNA (shctrl). (*Continued on the following page.*)

Published OnlineFirst November 10, 2020; DOI: 10.1158/0008-5472.CAN-20-1488

$r = 0.278$, $P < 0.0001$), and *Tp63* expression was positively associated with expression levels of genes related to glutathione metabolism, including GSS, GCLC, and SLC7A11 (Supplementary Fig. S8G–I, $P < 0.01$). Higher *Tp63* expression levels were also significantly associated with poor overall survival in this patient cohort (**Fig. 7M**, $P = 0.0431$). In all, our results support the existence of a "persister" cell population, marked by FZD7, metabolically characterized by increased glutathione-dependent antioxidant circuits and susceptible to ferroptosis. A potential mechanism leading to upregulation of GPX4 in platinum-tolerant ovarian cancer cells marked by FZD7 is engagement of Tp63, transactivated by β-catenin downstream of this receptor (**Fig. 7N**).

Discussion

Our data support that a Pt-T ("persister") cancer cell population serving as a reservoir for resistant tumors shares common features with CSCs and is characterized by *FZD7* expression. We demonstrate that the survival of these cells is dependent on an active FZD7–β-catenin–Tp63–GPX4 pathway, which renders these cells susceptible to inducers of ferroptosis. Our findings have several implications.

First, we identified FZD7 as a receptor enriched in Pt-T cancer cells and tumors. FZD7 is a transmembrane receptor that transduces signals involved in both the canonical and noncanonical Wnt pathways (36). Previous data indicated that FZD7 plays essential roles in stem cell biology and cancer (37). In breast and hepatocellular carcinoma, FZD7 has oncogenic functions, promoting cell proliferation, migration, and invasion (24, 38–41). Here we show that FZD7 marks a population representing ∼2% to 25% cells in Pt-T cell lines or tumors. The receptor's KD sensitized ovarian cancer cells to platinum, and its overexpression rendered cells resistant. Our group previously identified FZD7 as a receptor facilitating interaction of ovarian CSCs with the tumor niche (42) and the current findings corroborate the link between this receptor and cancer stemness. $FZD7^+$ cells were shown to proliferate more robustly as spheres, to express higher levels of stemness-associated TFs and display enhanced TIC. Interestingly, a related receptor, *FZD10,* was recently linked to PARP inhibitor resistance (43). Thus, it is likely that activation of the Wnt pathway through activation of one or more FZD receptors contributes to emergence of resistance to DNA-damaging agents.

Second, we report that FZD7 marks a population of cells highly susceptible to ferroptosis. Ferroptosis is a newly described type of cell death distinct from apoptosis and necrosis (44) characterized by iron-dependent accumulation of ROS resulting in increased lipid peroxidation and eventually leading to cell death (33). Ferroptosis is dependent on $NADPH/H^+$, polyunsaturated fatty acid metabolism, and the mevalonate and glutaminolysis metabolic pathways (31). Class 1 (system Xc^- inhibitors) and class 2 (GPX4) inhibitors are small molecules that induce ferroptosis (44). Here we observed that $FZD7^+$ platinum-tolerant cells were highly sensitive to ferroptosis induced by small molecules targeting GPX4. Tyrosine kinase inhibitor–tolerant cells have been reported to be sensitive to ferroptosis (3); however, no markers to identify cells prone to ferroptosis have been described.

Third, we found GPX4 to be significantly upregulated in Pt-T cells, xenografts, PDXs, and ovarian tumors residual after neoadjuvant chemotherapy. GPX4 detoxifies lipid peroxides (L-OOHs) by converting them to corresponding alcohols (L-OH), preventing the buildup of toxic, membrane oriented, lipid ROS (L-ROS; ref. 45). Aside from GPX4, other glutathione metabolism-related genes, such as *GSH* and *GSR,* are also involved in antioxidation defense. Cancer cells with acquired drug resistance were reported to have increased cellular GSH levels (46). Lower levels of endogenous ROS and higher levels of antioxidants and GSH were found in temozolomide (TMZ)-resistant glioblastoma cells (47) and silencing the GSH biosynthesis pathway triggered ferroptosis in clear cell carcinoma (48). Thus, modulation of redox homeostasis by GSH/GSR appears to be an important key modulating sensitivity of cancer cells to chemotherapy (47). Interestingly, in our study, the expression of glutathione metabolism-related genes *GSS, GSR, GPX2,* and *IDH* were directly correlated with expression of FZD7.

Lastly, our results shed light on a potential mechanism explaining the connection between FZD7 and activation of the glutathione regulatory machinery. A recent study reported that expression of GPX4 and of other genes involved in glutathione metabolism is regulated transcriptionally by *Tp63* (21). Tp63 (along with p53 and p73) belongs to the Tp53 family (49). TP63 regulates the self-renewal of progenitor cells in epithelial tissues through its by-product ΔNp63, which has dominant-negative effects on other p53 family isoforms and exerts tumorigenic functions (34). Unlike Tp53, inactivated in a majority of human cancers, including ovarian cancer, p63 is rarely mutated or inactivated. Overexpression of Tp63 was associated with poor survival in ovarian cancer (49, 50), similar to our findings exploring the TCGA database. *Tp63* was shown to regulate the expression of *FZD7* and enhance Wnt signaling in mammary tissue (49). A putative cross-talk between the Wnt/β catenin pathway and ΔNp63, the TP63 isoform lacking the N-terminus domain, was reported in skin, hair follicles, mammary glands, and limb buds during development (41). We observed a similar direct and strong correlation between *TP63* and *FZD7* expression in ovarian cancer cells, supporting that expression of this receptor is regulated by this TF. Furthermore, GPX4 expression, increased in FZD7-overexpressing cells, was downregulated by Tp63 knockdown, supporting this mechanism.

(*Continued.*) **D,** Western blot for β-catenin, P63, and GAPDH in SKOV3 and OVCAR5 cells transduced with shRNAs targeting *FZD7* (shFZD7) or control shRNA (shctrl). Quantification shows fold change of β-catenin and P63 expression across three experiments. **E** and **F,** *P63* mRNA levels (fold change ± SD, $n = 3$) in OVCAR5 (**E**) and SKOV3 (**F**) cells transfected with FZD7 vs. control vector (Ctrl). **G,** Western blot for β-catenin, P63, and GAPDH in OVCAR5 cells transfected with control (ctrl) or FZD7-pcDNA3.1 (FZD7). Quantification shows fold change of β-catenin and P63 expression across three experiments. **H,** Western blot for FZD7, β-catenin, P63, GPX4, and GAPDH in OVCAR5 cells transfected with shctrl, shFZD7 treated with WNT3a (150 ng/μL) and/or IWR-1-endo (1 μmol/L) for 24 hours ($n = 2$). **I–K,** *FZD7* (**I**), *P63* (**J**), and *GPX4* (**K**) mRNA expression levels (fold change ± SD, $n = 3$–4) in OVCAR5 cells transduced with control shRNAs (Ctrl_shctrl, Ctrl_shP63, FZD7_shctrl) or transfected with FZD7 expression vector and subsequently transduced with shRNA targeting *P63* (FZD7_shP63). For all comparisons: *, $P < 0.05$; **, $P < 0.01$; ***, $P < 0.001$. **L,** Scatter plot shows the correlation between *P63* and *FZD7 mRNA* expression levels in HGSOC tumors ($n = 419$) profiled in the TCGA database. Pearson correlation coefficients and *P* values are shown. **M,** Kaplan–Meier survival curves for HGSOC patients profiled in the TCGA having high ($n = 61$) or low ($n = 318$) *P63* (*TP63-012*) mRNA expression levels. High or low levels were defined based on statistically determined cutoff point that maximizes absolute value of the standardized two-sample linear rank statistic. **N,** Model demonstrates the proposed mechanism by which FZD7 engages the antioxidant pathway governed by GPX4.

Published OnlineFirst November 10, 2020; DOI: 10.1158/0008-5472.CAN-20-1488

In all, our results propose FZD7 as a new marker for cancer cell populations likely to survive exposure to platinum, enriched in antioxidant response mechanisms. These rare cells responsible for disease relapse after chemotherapy, share stemness features, and are susceptible to eradication through ferroptosis. Our data provide compelling evidence that targeting Pt-T FZD7^{+} cells by inducing ferroptosis is effective and could represent a new strategy in a disease of high unmet need.

Authors' Disclosures

E. Tanner reports personal fees from Merck and AstraZeneca outside the submitted work. R.V. Davuluri reports grants from National Library of Medicine during the conduct of the study. D. Matei reports grants from NCI and OCRA during the conduct of the study; personal fees from Astra Zenecca, GSK, Clovis, and Gynecologic Oncology Foundation outside the submitted work. No disclosures were reported by the other authors.

Authors' Contributions

Y. Wang: Conceptualization, data curation, software, formal analysis, validation, investigation, visualization, methodology, writing–original draft, writing–review and editing. **G. Zhao:** Data curation, software, formal analysis, validation, writing–original draft, writing–review and editing. **S. Condello:** Data curation. **H. Huang:** Data curation. **H. Cardenas:** Data curation, writing–review and editing. **E.J. Tanner:** Resources. **J. Wei:** Resources. **Y. Ji:** Software, formal analysis, methodology, writing–original draft. **J. Li:** Data curation, formal analysis, and validation. **Y. Tan:** Data curation, formal analysis, and validation. **R.V. Davuluri:** Software, formal analysis, supervision, and methodology. **M.E. Peter:** Resources, data curation, formal analysis, validation, methodology, writing–original draft, and writing–review and editing. **J.-X. Cheng:** Conceptualization, resources, data curation, formal analysis, supervision, funding acquisition, validation, investigation, methodology, writing–original draft, project administration, writing–review and editing. **D. Matei:** Conceptualization, resources, data curation, supervision, funding acquisition, investigation, methodology, writing–original draft, project administration, writing–review and editing.

Acknowledgments

This research was supported by funding from the Ovarian Cancer Research Alliance, the NCI (R01-CA224275), and the Diana Princess of Wales endowed Professorship from the Lurie Cancer Center to D. Matei and Friends of Prentice Award to S. Condello and D Matei. Tumor specimens were procured through the Tissue Pathology Core, and sequencing was performed in the NUSeq Core supported by NCI CCSG P30 CA060553 awarded to the Robert H Lurie Comprehensive Cancer Center. Flow cytometry analyses were performed in the Northwestern University–Flow Cytometry Core Facility supported by Cancer Center Support Grant NCI CA060553. This research was supported in part through the computational resources and staff contributions provided for the Quest high-performance computing facility at Northwestern University, which is jointly supported by the Office of the Provost, the Office for Research, and Northwestern University Information Technology.

The costs of publication of this article were defrayed in part by the payment of page charges. This article must therefore be hereby marked *advertisement* in accordance with 18 U.S.C. Section 1734 solely to indicate this fact.

Received May 4, 2020; revised October 3, 2020; accepted November 2, 2020; published first November 10, 2020.

References

1. Berek JS, Bertelsen K, du Bois A, Brady MF, Carmichael J, Eisenhauer EA, et al. Advanced epithelial ovarian cancer: 1998 consensus statements. Ann Oncol 1999;10:87–92.
2. Tummala MK, McGuire WP. Recurrent ovarian cancer. Clin Adv Hematol Oncol 2005;3:723–36.
3. Hangauer MJ, Viswanathan VS, Ryan MJ, Bole D, Eaton JK, Matov A, et al. Drug-tolerant persister cancer cells are vulnerable to GPX4 inhibition. Nature 2017;551:247–50.
4. Sharma SV, Lee DY, Li B, Quinlan MP, Takahashi F, Maheswaran S, et al. A chromatin-mediated reversible drug-tolerant state in cancer cell subpopulations. Cell 2010;141:69–80.
5. Liau BB, Sievers C, Donohue LK, Gillespie SM, Flavahan WA, Miller TE, et al. Adaptive chromatin remodeling drives glioblastoma stem cell plasticity and drug tolerance. Cell Stem Cell 2017;20:233–46.
6. Wang Y, Cardenas H, Fang F, Condello S, Taverna P, Segar M, et al. Epigenetic targeting of ovarian cancer stem cells. Cancer Res 2014;74:4922–36.
7. Wang Y, Zong X, Mitra S, Mitra AK, Matei D, Nephew KP. IL-6 mediates platinum-induced enrichment of ovarian cancer stem cells. JCI Insight 2018;3:e122360.
8. Zhang S, Balch C, Chan MW, Lai HC, Matei D, Schilder JM, et al. Identification and characterization of ovarian cancer-initiating cells from primary human tumors. Cancer Res 2008;68:4311–20.
9. Silva IA, Bai S, McLean K, Yang K, Griffith K, Thomas D, et al. Aldehyde dehydrogenase in combination with CD133 defines angiogenic ovarian cancer stem cells that portend poor patient survival. Cancer Res 2011;71:3991–4001.
10. Nguyen LV, Vanner R, Dirks P, Eaves CJ. Cancer stem cells: an evolving concept. Nat Rev Cancer 2012;12:133–43.
11. Nwani NG, Condello S, Wang Y, Swetzig WM, Barber E, Hurley T, et al. A novel ALDH1A1 inhibitor targets cells with stem cell characteristics in ovarian cancer. Cancers 2019;11:502.
12. Shi X, Zhang Y, Zheng J, Pan J. Reactive oxygen species in cancer stem cells. Antioxid Redox Signal 2012;16:1215–28.
13. Perets R, Wyant GA, Muto KW, Bijron JG, Poole BB, Chin KT, et al. Transformation of the fallopian tube secretory epithelium leads to high-grade serous ovarian cancer in Brca;Tp53;Pten models. Cancer Cell 2013;24:751–65.
14. Dong R, Qiang W, Guo H, Xu X, Kim JJ, Mazar A, et al. Histologic and molecular analysis of patient derived xenografts of high-grade serous ovarian carcinoma. J Hematol Oncol 2016;9:92.
15. Hu Y, Smyth GK. ELDA: extreme limiting dilution analysis for comparing depleted and enriched populations in stem cell and other assays. J Immunol Methods 2009;347:70–8.
16. Dobin A, Davis CA, Schlesinger F, Drenkow J, Zaleski C, Jha S, et al. STAR: ultrafast universal RNA-seq aligner. Bioinformatics 2013;29:7.
17. Li H, Handsaker B, Wysoker A, Fennell T, Ruan J, Homer N, et al. The sequence Alignment/Map format and SAMtools. Bioinformatics 2009;25:2078–9.
18. Anders S, Pyl PT, Huber W. HTSeq–a Python framework to work with high-throughput sequencing data. Bioinformatics 2015;31:166–9.
19. Robinson MD, McCarthy DJ, Smyth GK. edgeR: a Bioconductor package for differential expression analysis of digital gene expression data. Bioinformatics 2010;26:139–40.
20. Subramanian A, Tamayo P, Mootha VK, Mukherjee S, Ebert BL, Gillette MA, et al. Gene set enrichment analysis: a knowledge-based approach for interpreting genome-wide expression profiles. Proc Natl Acad Sci U S A 2005;102:15545–50.
21. Wang GX, Tu HC, Dong Y, Skanderup AJ, Wang Y, Takeda S, et al. DeltaNp63 inhibits oxidative stress-induced cell death, including ferroptosis, and cooperates with the BCL-2 family to promote clonogenic survival. Cell Rep 2017;21:2926–39.
22. Bicaku E, Xiong Y, Marchion DC, Chon HS, Stickles XB, Chen N, et al. In vitro analysis of ovarian cancer response to cisplatin, carboplatin, and paclitaxel identifies common pathways that are also associated with overall patient survival. Br J Cancer 2012;106:1967–75.
23. Asad M, Wong MK, Tan TZ, Choolani M, Low J, Mori S, et al. FZD7 drives in vitro aggressiveness in Stem-A subtype of ovarian cancer via regulation of non-canonical Wnt/PCP pathway. Cell Death Dis 2014;5:e1346.
24. Merle P, Kim M, Herrmann M, Gupte A, Lefrancois L, Califano S, et al. Oncogenic role of the frizzled-7/beta-catenin pathway in hepatocellular carcinoma. J Hepatol 2005;43:854–62.
25. Sakai W, Swisher EM, Jacquemont C, Chandramohan KV, Couch FJ, Langdon SP, et al. Functional restoration of BRCA2 protein by secondary BRCA2 mutations in BRCA2-mutated ovarian carcinoma. Cancer Res 2009;69:6381–6.

26. McMillen BD, Aponte MM, Liu Z, Helenowski IB, Scholtens DM, Buttin BM, et al. Expression analysis of MIR182 and its associated target genes in advanced ovarian carcinoma. Mod Pathol 2012;25:1644–53.
27. Gedye C, Sirskyj D, Lobo NC, Meens J, Hyatt E, Robinette M, et al. Cancer stem cells are underestimated by standard experimental methods in clear cell renal cell carcinoma. Sci Rep 2016;6:25220.
28. Liang H, Van Remmen H, Frohlich V, Lechleiter J, Richardson A, Ran Q. Gpx4 protects mitochondrial ATP generation against oxidative damage. Biochem Biophys Res Commun 2007;356:893–8.
29. Maiorino M, Conrad M, Ursini F. GPx4, lipid peroxidation, and cell death: discoveries, rediscoveries, and open issues. Antioxid Redox Signal 2018;29: 61–74.
30. Pan X, Lin Z, Jiang D, Yu Y, Yang D, Zhou H, et al. Erastin decreases radioresistance of NSCLC cells partially by inducing GPX4-mediated ferroptosis. Oncol Lett 2019;17:3001–8.
31. Seibt TM, Proneth B, Conrad M. Role of GPX4 in ferroptosis and its pharmacological implication. Free Radic Biol Med 2019;133:144–52.
32. Zou Y, Palte MJ, Deik AA, Li H, Eaton JK, Wang W, et al. A GPX4-dependent cancer cell state underlies the clear-cell morphology and confers sensitivity to ferroptosis. Nat Commun 2019;10:1617.
33. Sui X, Zhang R, Liu S, Duan T, Zhai L, Zhang M, et al. RSL3 drives ferroptosis through GPX4 inactivation and ROS production in colorectal cancer. Front Pharmacol 2018;9:1371.
34. Ruptier C, De Gasperis A, Ansieau S, Granjon A, Taniere P, Lafosse I, et al. TP63 P2 promoter functional analysis identifies beta-catenin as a key regulator of DeltaNp63 expression. Oncogene 2011;30:4656–65.
35. Cancer Genome Atlas Research Network. Integrated genomic analyses of ovarian carcinoma. Nature 2011;474:609–15.
36. Phesse T, Flanagan D, Vincan E. Frizzled7: a promising Achilles' heel for targeting the Wnt receptor complex to treat cancer. Cancers 2016;8:50.
37. King TD, Zhang W, Suto MJ, Li YH. Frizzled7 as an emerging target for cancer therapy. Cell Signal 2012;24:846–51.
38. Yang L, Wu X, Wang Y, Zhang K, Wu J, Yuan YC, et al. FZD7 has a critical role in cell proliferation in triple negative breast cancer. Oncogene 2011;30: 4437–46.
39. Wu W, Dang S, Feng Q, Liang J, Wang Y, Fan N. MicroRNA-542–3p inhibits the growth of hepatocellular carcinoma cells by targeting FZD7/Wnt signaling pathway. Biochem Biophys Res Commun 2017;482:100–5.
40. Ueno K, Hiura M, Suehiro Y, Hazama S, Hirata H, Oka M, et al. Frizzled-7 as a potential therapeutic target in colorectal cancer. Neoplasia 2008;10: 697–705.
41. Simmons GE, Pandey S, Nedeljkovic-Kurepa A, Saxena M, Wang A, Pruitt K. Frizzled 7 expression is positively regulated by SIRT1 and beta-catenin in breast cancer cells. PLoS One 2014;9:e98861.
42. Condello S, Sima L, Ivan C, Cardenas H, Schiltz G, Mishra RK, et al. Tissue tranglutaminase regulates interactions between ovarian cancer stem cells and the tumor niche. Cancer Res 2018;78:2990–3001.
43. Fukumoto T, Zhu H, Nacarelli T, Karakashev S, Fatkhutdinov N, Wu S, et al. N(6)-methylation of adenosine of FZD10 mRNA contributes to PARP inhibitor resistance. Cancer Res 2019;79:2812–20.
44. Yu H, Guo P, Xie X, Wang Y, Chen G. Ferroptosis, a new form of cell death, and its relationships with tumourous diseases. J Cell Mol Med 2017;21:648–57.
45. Forcina GC, Dixon SJ. GPX4 at the crossroads of lipid homeostasis and ferroptosis. Proteomics 2019;19:e1800311.
46. Chen HH, Kuo MT. Role of glutathione in the regulation of Cisplatin resistance in cancer chemotherapy. Met Based Drugs 2010;2010:430939.
47. Zhu Z, Du S, Du Y, Ren J, Ying G, Yan Z. Glutathione reductase mediates drug resistance in glioblastoma cells by regulating redox homeostasis. J Neurochem 2018;144:93–104.
48. Miess H, Dankworth B, Gouw AM, Rosenfeldt M, Schmitz W, Jiang M, et al. The glutathione redox system is essential to prevent ferroptosis caused by impaired lipid metabolism in clear cell renal cell carcinoma. Oncogene 2018; 37:5435–50.
49. Chakrabarti R, Wei Y, Hwang J, Hang X, Andres Blanco M, Choudhury A, et al. DeltaNp63 promotes stem cell activity in mammary gland development and basal-like breast cancer by enhancing Fzd7 expression and Wnt signalling. Nat Cell Biol 2014;16:1004–15.
50. Marchini S, Marabese M, Marrazzo E, Mariani P, Cattaneo D, Fossati R, et al. Delta Np63 expression is associated with poor survival in ovarian cancer. Ann Oncol 2008;19:501–7.

Published OnlineFirst November 10, 2020; DOI: 10.1158/0008-5472.CAN-20-1488

Frizzled-7 Identifies Platinum-Tolerant Ovarian Cancer Cells Susceptible to Ferroptosis

Yinu Wang, Guangyuan Zhao, Salvatore Condello, et al.

Cancer Res 2021;81:384-399. Published OnlineFirst November 10, 2020.